Citric Acid-Assisted Hydrothermal Synthesis of Luminescent $TbPO_4$:Eu Nanocrystals: Controlled Morphology and Tunable Emission

Weihua Di,*,†,‡ Marc-Georg Willinger,† Rute A. S. Ferreira,§ Xinguang Ren,‡ Shaozhe Lu,‡ and Nicola Pinna*,†

Department of Chemistry, CICECO, University of Aveiro, 3810-193 Aveiro, Portugal, Key Laboratory of Excited-state Processes, Changchun Institute of Optics, Fine Mechanics and Physics, Chinese Academy of Sciences, Changchun 130033, P.R. China, and Department of Physics, CICECO, University of Aveiro, 3810-193 Aveiro, Portugal

Received: August 22, 2008; Revised Manuscript Received: September 26, 2008

This work reports a simple hydrothermal route using citric acid as a "shape modifier" for the controlled synthesis of luminescent $TbPO_4$:Eu nanocrystals. The size and morphology of products change remarkably when the proportion of citric acid involved in the reaction increases. The multiple roles that citric acid plays during the controlled synthesis are discussed to try to understand the crystallization and growth dynamics of $TbPO_4$ crystals. The photoluminescence properties of $TbPO_4$:Eu are investigated. The excitation spectra and the variation of the $^5D_4$ lifetime values as a function of the Eu^{3+} concentration points out the occurrence of Tb^{3+}-to-Eu^{3+} energy transfer, resulting in a maximum absolute emission quantum yield of 0.14. The possibility to tune the size, the shape, and the optical properties of the nanocrystals reported in this work might be useful for applications in optoelectronics or biolabeling. Moreover, this simple approach might also be applied for the synthesis of other luminescent phosphates.

Introduction

In recent decades, numerous efforts have been devoted to the development of synthesis approaches of nanostructures with control over size and shape. These methods include gas-phase syntheses (e.g., vapor−liquid−solid process,[1,2] chemical vapor deposition,[3,4] molecular beam epitaxy,[5] and spray pyrolysis[6]) and liquid-phase syntheses in aqueous or nonhydrolytic media. Liquid-phase approaches are recognized to be versatile and suitable for the reproducible synthesis of a large variety of nanomaterials.[7−16]

In solution syntheses, the control of particles size and shape at the nanometer level is commonly achieved by using organic molecules (e.g., surfactants). The main drawback, resulting from surface-absorbed surfactants, is the diminished accessibility of the particles surface, which is a serious issue regarding applications in gas sensing or catalysis. For example, the commonly used trioctylphosphine oxide starts to decompose at around 425 °C.[17] Since catalytic activity strongly depends on the size, shape, and especially the exposed facets of the material,[18] the ability to control their growth without the use of surfactants is eagerly needed.

For this purpose, the approach of using simpler and more easily removable organic molecules acting as solvent or reactant and/or as ligand for the control of the crystal size and shape is a possible solution to overcome the specific drawbacks of the surfactant-assisted routes. For example, the rapidly growing number of inorganic nanoparticles that were prepared by nonaqueous and/or nonhydrolytic processes in organic solvents without the application of surfactants clearly indicates that these are valuable alternatives.[7,19] The use of ionic liquids as organic solvents constitutes another fast-developing research field, which enables the synthesis of various inorganic nanoparticles and nanostructures either in the presence or under exclusion of water.[20−23] Small chelating ligands such as citric acid have already been used as "shape modifiers" to adjust and control the size and morphology of the products.[24,25] These organic molecules are known to dynamically modify the crystal growth by either promoting or inhibiting the crystal growth along specific crystallographic facets. Through properly choosing organic additives that might have specific molecular complementarity with their inorganic counterparts, the growth of inorganic crystals can be rationally directed to yield products with desirable morphologies and/or hierarchical structures.[26]

Rare earth orthophosphates ($REPO_4$) represent an important family of materials, and they have been used as active components in a wide range of applications such as phosphors, sensors, catalysts, proton conductors, ceramic materials, biolabeling, and phototherapy.[27−32] In recent years, much effort has been devoted to tailoring the size and morphology of $REPO_4$ and to optimize the optical properties. Hasse and co-workers obtained $REPO_4$ nanocrystals dispersions with good optical properties using a surfactant-assisted route.[33] Feldmann and coworker synthesized luminescent $LaPO_4$:Ce,Tb nanoparticles with a high quantum yield using a microwave-assisted synthesis method with ionic liquids as the reaction media.[34] Yan and coworkers recently reported on the synthesis of aligned and highly luminescent monodisperse $REPO_4$ nanocrystals by a limited anion-exchange reaction in solution phase.[35] However, there are still few reports on the controlled synthesis of $REPO_4$ nanocrystals with tunable morphologies and emissions. In this work, we choose to synthesize Eu^{3+}-doped $TbPO_4$ nanocrystals for two specific reasons. On the one hand, we attempted to control the size, morphology, and crystallinity of $TbPO_4$:Eu nanocrystals by the use of an organic additive (citric acid, CA) and try to understand its role in the growth of $TbPO_4$:Eu crystals. On the

* To whom correspondence should be addressed. E-mail: pinna@ua.pt (N.P.); weihuadi@ua.pt (W.D.). Fax: +351 234370004.
† Department of Chemistry, CICECO, University of Aveiro.
‡ Chinese Academy of Sciences.
§ Department of Physics, CICECO, University of Aveiro.

10.1021/jp807527y CCC: $40.75
Published on Web 11/11/2008

other hand, Tb^{3+} and Eu^{3+} in some crystalline modifications of rare earth orthophosphates are themselves excellent green and red light emitting centers, respectively. The presence of energy transfer between the Tb^{3+} excited states and those of Eu^{3+} allows the fine-tuning of the emission chromaticity by changing either the Tb/Eu ratio or the excitation wavelength. Moreover, an increase in the absolute emission quantum yield was found for the doped samples relative to that of the pure $TbPO_4$ material.

Experimental Methods

Rare earth nitrate ($Tb(NO_3)_3$ and $Eu(NO_3)_3$) stock solutions of 0.2 M were prepared by dissolving the corresponding metal oxide in concentrated HNO_3 at elevated temperature. Tb_4O_7 (99.99%) and Eu_2O_3 (99.99%) were purchased from Shanghai Yuelong New Materials Co., Ltd., and other chemicals were purchased from Beijing Chemical Co. All chemicals were analytical grade reagents and used directly without further purification. In a typical procedure using citric acid (CA) as ligand, 20 mL of $Tb(NO_3)_3$ (0.2 M) solution was added to 20 mL of aqueous solution containing 8 mmol of citric acid. The solution, turning turbid due to the formation of the terbium citrate complex, was kept under vigorous stirring for 30 min. Subsequently, an aqueous solution containing 4.4 mmol of $(NH_4)_2HPO_4$ was added. The final pH of the mixture was adjusted to about 1−2 by adding aqueous ammonia (NH_4OH). After additional agitation for 15 min, the solution was transferred into a Teflon bottle held in a stainless steel autoclave, which was sealed and heated at 150 °C for 20 h. After cooling down the autoclave to room temperature, the precipitation was separated by centrifugation, washed with deionized water and ethanol several times, and finally dried overnight under air at 60 °C. Samples with different molar ratios of CA/Re^{3+} (1:0.2, 1:0.8, 1:1.2, 1:8) were synthesized according to the same procedure; only the amount of CA was modified. For the synthesis without citric acid ligand, 40 mL of aqueous solution of 4.4 mmol of $(NH_4)_2HPO_4$ was added directly into 20 mL of $Tb(NO_3)_3$ solution. The other preparation condition and parameters were kept constant. Eu^{3+}-doped terbium phosphate samples were obtained under the same conditions by replacing a fraction of $Tb(NO_3)_3$ by $Eu(NO_3)_3$.

The X-ray powder diffraction (XRD) data were collected on an X'Pert MPD Philips diffractometer (Cu Kα X-radiation at 40 kV and 50 mA). The patterns were measured in the 2θ range from 10° to 70° with a scanning step of 0.02°.

Scanning electron microscopy (SEM) images were recorded using a FEG-SEM Hitachi SU-70 microscope operating at 4 kV at a working distance of 2−3 mm. For the SEM observations, samples were prepared without any carbon coating simply by depositing some powder onto a double gluing tape. High-resolution transmission electron microscopy (HRTEM) investigations were carried using a JEOL 2200FS microscope. Samples for TEM investigations were prepared by first dispersing the particles in ethanol under assistance of ultrasonification and then dropping 1 drop of the suspension on a copper TEM grid coated with a holey carbon film.

The luminescence in the ultraviolet/visible (UV/vis) spectral range was recorded between 12 K and room temperature with a modular double grating excitation spectrofluorimeter with a TRIAX 320 emission monochromator (Fluorolog-3, Jobin Yvon-Spex) coupled to a R928 Hamamatsu photomultiplier, using the front face acquisition mode. The excitation source was a 450 W Xe arc lamp. The emission spectra were corrected for detection and optical spectral response of the spectrofluorimeter and the excitation spectra were corrected for the spectral distribution of the lamp intensity using a photodiode reference detector. Fluorescent lifetime measurements were made under a pulsed excitation at 355 nm from the third harmonic of a Nd:YAG laser. It was with a line width of 1.0 cm^{-1}, pulse duration of 10 ns, and repetition frequency of 10 Hz.

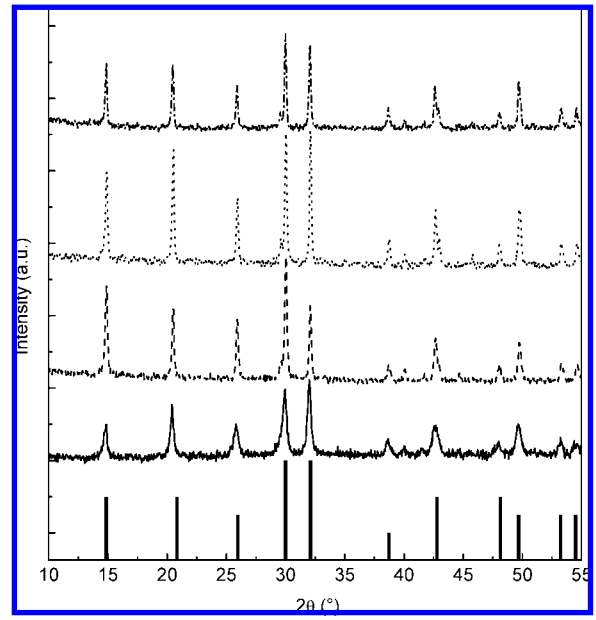

Figure 1. XRD patterns of the as-synthesized samples without CA (full line) and with CA:Tb = 0.2:1 (dashed line), CA:Tb = 0.8:1 (dotted line), and CA:Tb = 2:1 (dash-dotted line) ligand to metal ratios. Vertical bars denote the peak positions and relative intensities of the rhabdophane structure (JCPDS card No. 20-1244).

The absolute emission quantum yields were measured at room temperature using a quantum yield measurement system C9920-02 from Hamamatsu with a 150 W xenon lamp coupled to a monochromator for wavelength discrimination, an integrating sphere as a sample chamber, and a multichannel analyzer for signal detection. Three measurements were made for each sample so that the average value is reported. The method is accurate to within 10%. The samples for luminescence studies were previously calcined at 500 °C for 90 min to remove water from the structure (cf. thermal analysis in Figure SI-2).

Results and Discussion

Structure and Morphology. The structure and crystallinity of the products were studied by XRD. Figure 1 shows the XRD patterns of the as-synthesized samples for different CA:Tb ratios. All the as-synthesized samples are crystalline and show diffraction peaks that can be safely indexed to the hexagonal rhabdophane-type $TbPO_4$ hydrate ($TbPO_4$:H_2O) phase (JCPDS card No. 20-1244). No additional diffractions that could be attributed to impurities are observed.

The sample synthesized without CA in general presents broader diffractions denoting a smaller size. The evaluation of the average size from XRD patterns denotes that the size along the [100] direction increases with the amount of citric acid. As discussed later (cf. TEM study), this particular direction correspond to the width of the nanorods.

The size and morphology of the samples were characterized by scanning electron microscopy (SEM) and transmission electron microscopy (TEM). Figures 2 and 3 present the SEM images of several samples synthesized for different CA:Tb ratios. In the absence of CA, the sample is composed of bundles

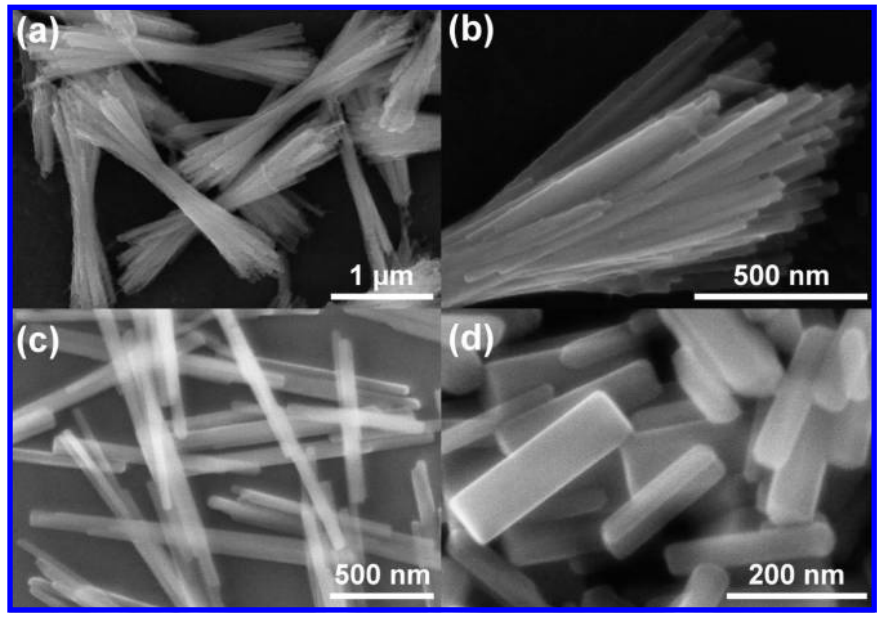

Figure 2. SEM images of the as-synthesized samples (a,b) without CA and with (c) CA:Tb = 0.2:1 and (d) CA:Tb = 0.8:1 ligand to metal ratios.

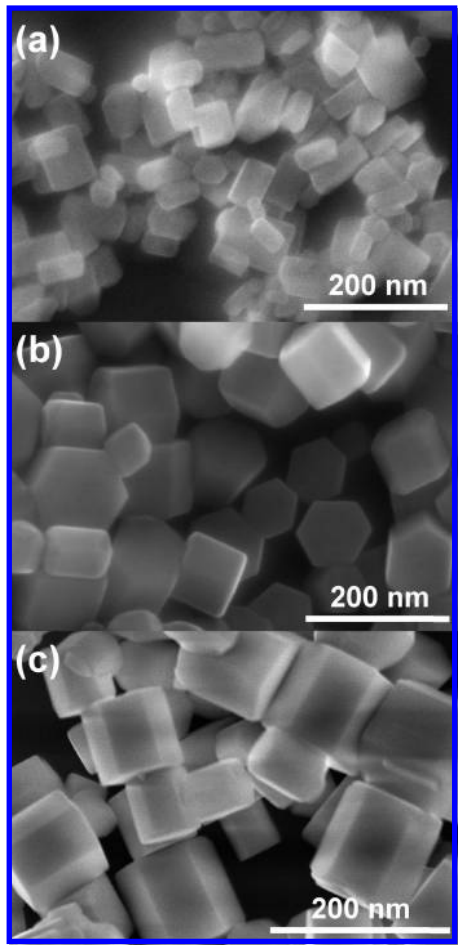

Figure 3. SEM images of the as-synthesized samples with (a) CA:Tb = 1.2:1, (b) CA:Tb = 2:1, and (c) CA:Tb = 8:1 ligand to metal ratios.

of nanorods with a high aspect ratio, measuring 2−3 μm in length and about 20−30 nm in width (Figure 2a,b).

The addition of CA dramatically affects the final morphology of the particles. Indeed, even a small amount (CA:Tb = 0.2:1) permits the synthesis of well-isolated nanorods with a slightly shorter length (1−1.5 μm) but larger width (40−50 nm) and, hence, a smaller aspect ratio (Figure 2c). A further increase of CA leads to the formation of rectangular nanoprisms with even smaller aspect ratio, measuring around 200 nm in length at a width of 50−60 nm (Figure 2d). For CA concentrations higher than Tb a new morphology appears. Indeed, the sample consists of a mixture of rectangular and hexagonal nanoprisms for a concentration ratio of CA:Tb = 1.2:1 (Figure 3a). For larger concentrations only hexagonal nanoprisms are observed (Figure 3b,c). The particles generally are well-faceted and show a highly symmetric shape, indicating that they are monocrystalline. The good agreement between the width extracted from the XRD studies and the SEM images supports this observation (cf. Table 1).

TABLE 1: Nanoparticle Widths Evaluated Using the Sherrer Equation from the (100) Diffraction Peaks, for Different Citric Acid Concentrations

molar ratio CA:Tb^{3+}	size (nm)
0:1	29.9
0.2:1	44.0
0.8:1	46.0
2:1	52.7

A deeper insight into the crystalline quality, preferential growth axis, and the exposed facets of the particles is obtained from high-resolution TEM (HRTEM) studies. Figure 4 shows HRTEM micrographs recorded from samples with a growing CA:Tb ratio.

All observed particles are single-crystalline, revealing lattice fringes that are in agreement with the corresponding lattice planes of the terbium phosphate hydrate phase that was also found by XRD. Without CA and at small CA concentrations, the growth of the particles proceeds mainly along the *c*-axis ⟨001⟩, leading to the observed rod-shaped particles with high aspect ratio. As the CA concentration increases, the growth rate along the ⟨001⟩ direction decreases. Already at a CA:Tb concentration of 0.8:1 additional facets due to the exposure of {012} and, less frequently, {021} planes can be observed (see Figure 4c). Obviously, one of the consequences of the presence

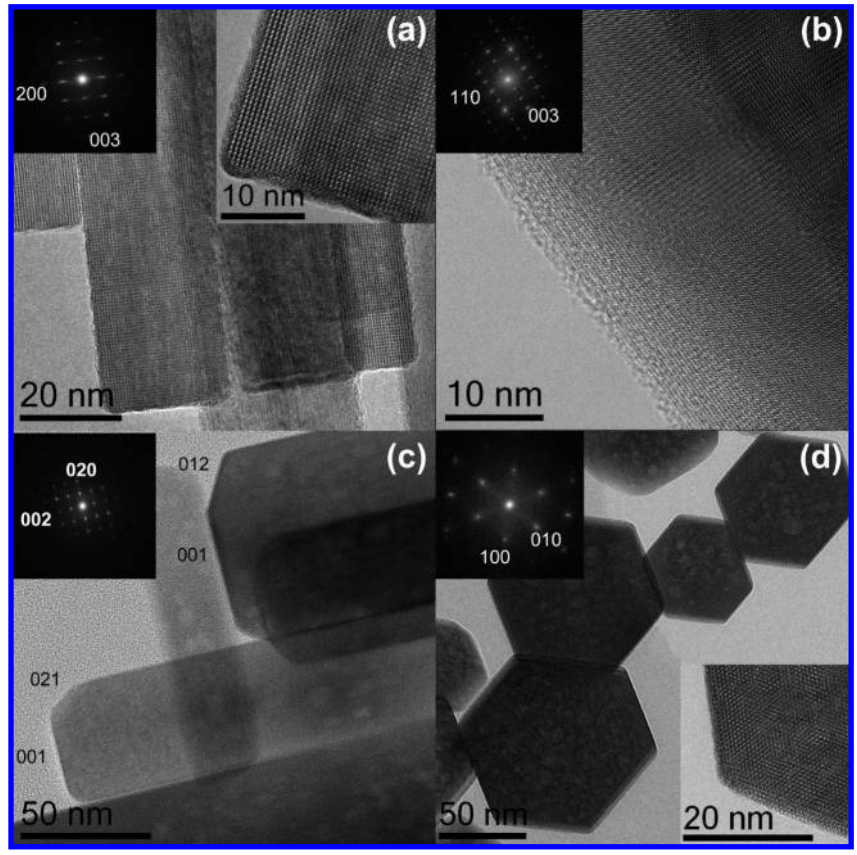

Figure 4. HRTEM images recorded from as-synthesized samples: (a) without CA, (b−d) with a ligand to metal ratio of respectively 0.2:1, 0.8:1, and 2:1. In (c) the Miller indices of some facets are shown.

of CA is the inibition of the ⟨001⟩ growth direction and the resulting relative enhancement of the growth sideways along the ⟨100⟩ and ⟨010⟩ directions. In addition to that, there might also be some direct mechanisms involved in which the CA accelerates the growth along these directions and the formation of more defined faces. Finally, at a CA:Tb concentration of 2:1, the ⟨001⟩ direction no longer dominates as the main growth direction and an increased, homogeneous growth along the ⟨100⟩ and ⟨010⟩ directions leads to highly symmetric hexagonal nanoprisms with well-defined crystallographic facets (see Figure 4d).

The above results indicate that the CA influences considerably the growth of $TbPO_4$ crystals. CA should play multiple roles during the entire course of the synthesis. CA possesses three carboxylic acid and one hydroxyl functional groups, providing chelating ability. During the reaction, CA reacts with Tb^{3+} ions, at first, to form citrate complexes. This is traduced by the formation of a milky suspension when the aqueous solutions containing Tb^{3+} and CA are mixed. After the addition of the phosphorus source $(NH_4)_2HPO_4$, an ion-exchange reaction between PO_4^{3-} and citrate ions takes place under hydrothermal conditions, leading to the formation of $TbPO_4$. The nucleation rate is certainly modified by the presence of citrate complexes. Moreover, during the growth process, citrate ions can also selectively bind to specific crystallographic facets as it was already reported in other studies.[25,36] Such a preferential adsorption can effectively restrict or promote the growth along specific directions, leading to dramatic modifications on the final shape of the crystals. Up to now, it is not exactly known how CA controls the final crystal morphology from nanorods to highly symmetric hexagonal nanoprisms. On the other hand, it is clear that its chelating property and its preferential adsorption onto certain facets should both influence the nucleation and growth of $TbPO_4$ and finally permit a precise tuning of the final crystal morphology.

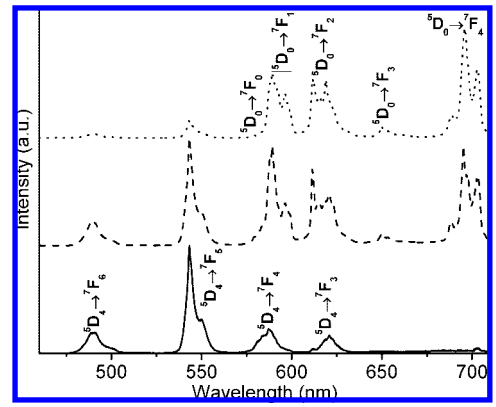

Figure 5. Room temperature emission spectra of pure (full line) and Eu^{3+}-doped $TbPO_4$ (0.1 dashed line and 0.3 mol % dotted line) excited at 377 nm.

Photoluminescence. Figure 5 presents the emission spectra of pure $TbPO_4$ and $TbPO_4$ doped with 0.1 and 0.3% of Eu^{3+}. When the pure $TbPO_4{:}H_2O$ nanoparticles are excited in the UV (377 nm), the spectrum displays a series of emission lines ascribed to the Tb^{3+} intra-$4f^8$ $^5D_4 \rightarrow {}^7F_{6-3}$ electronic transitions. Doping with small amounts of europium leads to additional emission lines appearing from 585 to 710 nm ascribed to the Eu^{3+} intra-$4f^6$ $^5D_0 \rightarrow {}^7F_{0-4}$ transitions. The simultaneous observation of the emission arising from Tb^{3+} and Eu^{3+} excited states suggests the existence of Tb^{3+}-to-Eu^{3+} energy transfer, as we will demonstrate next.

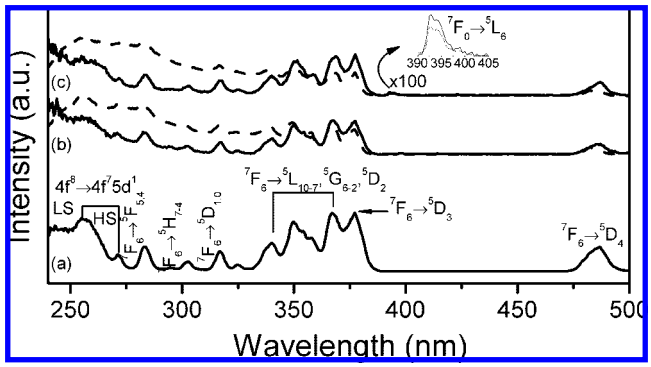

Figure 6. Room temperature (full line) and 12 K (dashed line) excitation spectra of the (a) pure $TbPO_4$ monitored at 543 nm and of the Eu^{3+}-doped $TbPO_4$ (0.3 mol %) monitored at (b) 543 nm and (c) 611 nm. The inset shows a magnification of the $^7F_0 \rightarrow {}^5L_6$ transition for the Eu^{3+}-doped $TbPO_4$ (0.3 mol %) monitored at 611 nm.

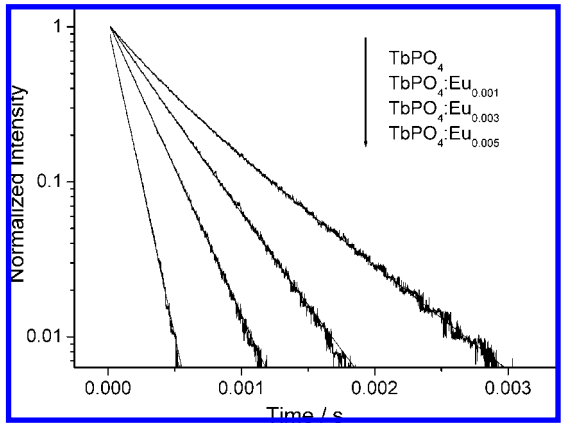

Figure 7. Room temperature emission decay curves of $TbPO_4$ doped with different Eu^{3+} concentrations monitored at 543 nm.

Figure 6 shows the room temperature excitation spectrum of the undoped $TbPO_4$ sample monitored within the $^5D_4 \rightarrow {}^7F_5$ transition. The bands centered at 240 and 250−270 nm are assigned to the spin-allowed (low-spin, LS) and spin-forbidden (high-spin, HS) interconfigurational Tb^{3+} fd transitions, respectively, and the remaining peaks are assigned to intra-$4f^8$ transitions between the $^7F_6$ and the $^5F_{5,4}$, $^5H_{7-4}$, $^5D_{1,0}$, $^5L_{10-7}$, $^5G_{6-2}$, and $^5D_{2-4}$ levels.

The excitation of the Eu-doped samples was monitored within the Tb^{3+} $^5D_4 \rightarrow {}^7F_5$ (544 nm) and Eu^{3+} $^5D_0 \rightarrow {}^7F_4$ (697 nm) transitions. The former excitation spectra is similar to the one acquired for the undoped $TbPO_4$ sample. The spectra monitored within the Eu^{3+} emission lines exhibit a series of Tb^{3+} related transitions and a low relative intensity peak attributed to the Eu^{3+} $^7F_0 \rightarrow {}^5L_6$ transition (inset of Figure 6). The observation of the Tb^{3+} excited levels in the excitation spectra monitored within the Eu^{3+} intra-$4f^6$ transitions is a clear evidence of the occurrence of Tb^{3+}-to-Eu^{3+} energy transfer. The spectra acquired at 11 K are similar to those measured at room temperature, indicating that the Tb^{3+}-to-Eu^{3+} energy transfer is active in this temperature interval.

The existence of the energy transfer from Tb^{3+}-to-Eu^{3+} can also be evidenced by the dependence of the $^5D_4$ lifetime values on the Eu^{3+} concentration. Figure 7 reports the $^5D_4$ emission decay curves of pure $TbPO_4$ and doped $TbPO_4$ by monitoring the Tb^{3+} emission at 543 nm. All the curves are well-reproduced by a single exponential function, yielding to lifetime values of 0.495 ± 0.001 ms for the pure $TbPO_4$ sample and 0.3535 ± 0.001, 0.230 ± 0.001, and 0.109 ± 0.001 ms for the Eu^{3+}-doped $TbPO_4$ with 0.1, 0.3, and 0.5 mol %, respectively.

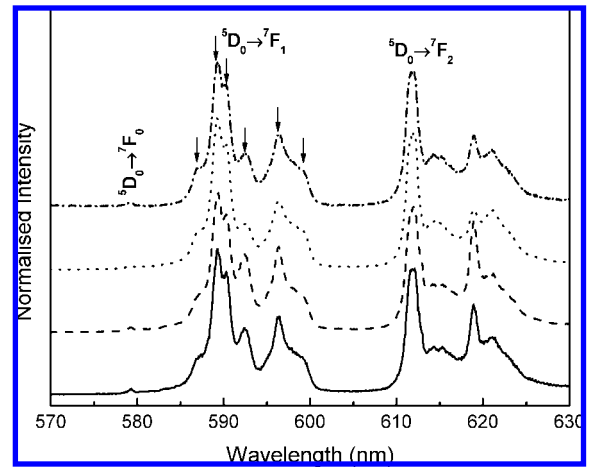

Figure 8. Low-temperature (11 K) emission spectra of $TbPO_4$:$Eu_{0.003}$ excited at 255 nm (solid line), 281 nm (dashed line), 366 nm (dotted line), and 393 nm (dash-dotted line).

The decrease of the $^5D_4$ lifetime value as the amount of Eu^{3+} increases is in good agreement with the presence of Tb^{3+}-to-Eu^{3+} energy transfer.

It is well-known that the lifetime of the $^5D_3$ state is much shorter than that of the $^5D_4$ state, leading to very quick relaxation from $^5D_3$ to $^5D_4$ levels.[37,38] This indicates that the energy transfer taking place from the Tb^{3+} $^5D_4$ should be one of the preferential paths.

To obtain further insight into the Eu^{3+} local coordination, higher resolution spectra of the Eu^{3+} emission were acquired at 11 K under different excitation wavelengths. As Figure 8 evidences, there are six components for the Eu^{3+} $^5D_0 \rightarrow {}^7F_1$ transition, whose maximum splitting allowed for a single Eu^{3+} local environment, is 3 ($2J + 1$). This observation clearly points out the presence of more than one local Eu^{3+} site. Comparison of these findings with structural data is not possible as no accurate description of the structure of the rhabdophane-type $TbPO_4$ hydrate phase (i.e., precise atomic positions) is reported. On the other hand, this result, proving that two nonequivalent coordination sites exist in the structure, could help in upcoming structure refinements, using Eu^{3+} as a local probe.

The photoluminescence features were further quantified through the estimation of the absolute emission quantum yield as a function of the excitation wavelength and Eu^{3+} concentration. For all the samples, the maximum quantum yield value was attained at 377 nm excitation wavelength, being 0.07 for the pure $TbPO_4$ sample and 0.12−0.14 for the Eu^{3+}-doped ones. Under direct intra-$4f^6$ excitation ($^5L_6$, 393 nm) the quantum yield value of the $TbPO_4$:Eu samples lies below the detection limits of our equipment (0.001), confirming that the preferential path for the Eu^{3+} excitation is via the Tb^{3+} excited levels.

The above-mentioned quantum yield values are similar to those reported for colloidal solutions of $LaPO_4$:Eu (0.10) and $CePO_4$:Tb (0.11−0.16) nanoparticles[39] and for $CePO_4$:Tb nanorods (0.17).[40] Typically, such low values are attributed to the presence of nonradiative transition channels mediated via a high surface-to-volume ratio existent in nanoparticles. To minimize those effects, synthesis strategies involving both the nanoparticle surface modification and the enhancement of the crystanility have been proposed.[33,34,40,41]

Conclusions

In this work a hydrothermal route making use of citric acid for the synthesis of hydrated $TbPO_4$:Eu nanocrystals with

controlled morphologies and tunable photoluminescence properties is reported. Multiple roles can be attributed to citric acid (CA) during the entire course of the synthesis: (i) CA serves as ligand and chelating agent of the Tb^{3+} ions. It permits achieving control over the nucleation rate and obtaining samples of low polydispersity, (ii) CA seems to preferentially inhibit the growth along the [001] axis of the $TbPO_4$ crystals. Furthermore, there is an effect on the growth speed along the [100] and [010] directions, opening the possibility of controlling the final morphology of the nanocrystals. As a function of the CA concentration, the nanocrystal shape evolves from bundle-like aggregates composed of nanorods to well-dispersed nanorods, rectangular nanoprisms, and finally to hexagonal nanoprisms.

The nanocrystals were successfully doped with Eu^{3+}. Upon excitation over a large energy range, emissions of both ions Tb^{3+} and Eu^{3+} intra-4f emission lines could be observed. This is due to an efficient energy transfer from Tb^{3+} to Eu^{3+}, which takes place from the Tb^{3+} $^5D_4$ states to the Eu^{3+} levels. The efficient Tb^{3+}-to-Eu^{3+} energy transfer can be successfully used to tune the emission color by simply changing the concentration of europium. It can be potentially used in three-color-based displays and white light illumination applications. Finally, we do not see any impediment in the application of the present approach to additional luminescent phosphates.

Acknowledgment. This work was partially supported by the National Natural Science Foundation of China (Grant No. 50502031), Natural Science Foundation of Jilin Province (Grant No. 20060522), FCT Project No. (PTDC/CTM/65667/2006) and Grant No. (SFRH/BPD/40881/2007), and FAME network of excellence. W.D. is grateful for the special starting research fund for the Awardees of President Prize of Chinese Academy of Sciences (2008−2009).

Supporting Information Available: This material is available free of charge via the Internet at http://pubs.acs.org.

References and Notes

(1) Saito, Y.; Matsumoto, T. *Nature* **1998**, *392*, 237.
(2) Xia, Y.; Yang, P.; Sun, Y.; Wu, Y.; Mayers, B.; Gates, B.; Yin, Y.; Kin, F.; Yan, H. *Adv. Mater.* **2003**, *15*, 353.
(3) Kong, W. Y.; Ding, Y.; Yang, R. S.; Wang, Z. L. *Science* **2004**, *303*, 1348.
(4) Duan, X.; Lieber, C. M. *Adv. Mater.* **2000**, *12*, 198.
(5) Ploog, K. H. *J. Cryst. Growth* **2007**, *301*, 10.
(6) Strobel, R.; Pratsinis, S. E. *J. Mater. Chem.* **2007**, *17*, 4743.
(7) Pinna, N.; Niederberger, M. *Angew. Chem., Int. Ed.* **2008**, *47*, 5292.
(8) Park, J.; Joo, J.; Kwon, S. G.; Jang, Y.; Hyeon, T. *Angew. Chem.* **2007**, *46*, 4630.
(9) Jun, Y. W.; Choi, J. S.; Cheon, J. *Angew. Chem., Int. Ed.* **2006**, *45*, 3414.
(10) Zhang, D. F.; Sun, L. D.; Yin, J. L.; Yan, C. H. *Adv. Mater.* **2003**, *15*, 1022.
(11) Pinna, N. *J. Mater. Chem.* **2007**, *17*, 2769.
(12) Di, W. H.; Wang, X. J.; Chen, B. J.; Lu, S. Z.; Zhao, X. X. *J. Phys. Chem. B* **2005**, *109*, 13154.
(13) Mai, H. X.; Zhang, Y. W.; Si, R.; Yan, Z. G.; Sun, L. D.; You, L. P.; Yan, C. H. *J. Am. Chem. Soc.* **2006**, *128*, 6426.
(14) Riwotzki, K.; Meyssamy, H.; Schnablegger, H.; Kornowski, A.; Haase, M. H. *Angew. Chem., Int. Ed.* **2001**, *40*, 573.
(15) Puntes, V. F.; Krishnan, K. M.; Alivisatos, A. P. *Science* **2001**, *291*, 2115.
(16) Kim, Y. H.; Jun, Y.; Jun, B. H.; Lee, S. M.; Cheon, J. *J. Am. Chem. Soc.* **2002**, *124*, 12656.
(17) Foos, E. E.; Wilkinson, J.; Makinen, A. J.; Watkins, N. J.; Kafafi, Z. H.; Long, J. P. *Chem. Mater.* **2006**, *18*, 2886.
(18) Schlogl, R.; Hamid, S. *Angew. Chem., Int. Ed.* **2004**, *43*, 1628.
(19) Niederberger, M.; Garnweitner, G.; Pinna, N.; Neri, G. *Prog. Solid State Chem.* **2005**, *33*, 59.
(20) Antonietti, M.; Kuang, D. B.; Smarsly, B.; Yong, Z. *Angew. Chem., Int. Ed.* **2004**, *43*, 4988.
(21) Dobbs, W.; Suisse, J. M.; Douce, L.; Welter, R. *Angew. Chem., Int. Ed.* **2006**, *45*, 4179.
(22) Kaper, H.; Endres, F.; Djerdj, L.; Antonietti, M.; Smarsly, B. M.; Maier, J.; Hu, Y. S. *Small* **2007**, *3*, 1753.
(23) Endres, F.; Abedin, S. *Phys. Chem. Chem. Phys.* **2006**, *8*, 2101.
(24) Sun, Y.; Xia, Y. *Science* **2002**, *298*, 2176.
(25) Kilin, D. S.; Prezhdo, O. V.; Xia, Y. N. *Chem. Phys. Lett.* **2008**, *458*, 113.
(26) Wang, X.; Zhuang, J.; Peng, Q.; Li, Y. D. *Adv. Mater.* **2006**, *18*, 2031.
(27) Lehmann, O.; Kompe, K.; Haase, M. *J. Am. Chem. Soc.* **2004**, *126*, 14935.
(28) Blasse, G.; Grabmaier, B. C. *Luminescent Materials*; Springer: Berlin, 1994.
(29) Pellegrino, T.; Kudera, S.; Liedl, T.; Javier, A. M.; Manna, L.; Parak, W. *Small* **2005**, *1*, 48.
(30) Kim, S.; Lim, Y. T.; Soltesz, E. G.; DeGrand, A. M.; Lee, J.; nakayama, A.; Parker, J. A.; Mihaljevic, T.; Laurence, R. G.; Dor, D. M.; Cohn, L. H.; Bawendi, M. G.; Frangioni, J. V. *Nat. Biotechnol.* **2003**, *22*, 93.
(31) Dubertret, B.; Skourides, P.; Norris, D. J.; Noireaux, V.; Brivanloue, A. H.; Libchaber, A. *Science* **2002**, *298*, 1759.
(32) Justel, T.; Nikol, H.; Ronda, C. *Angew. Chem., Int. Ed.* **1998**, *37*, 3084.
(33) Kompe, K.; Borchert, H.; Storz, J.; Lobo, A.; Adam, S.; Moller, T.; Hasse, M. *Angew. Chem., Int. Ed.* **2003**, *42*, 5513.
(34) Buehler, G.; Feldmann, C. *Angew. Chem., Int. Ed.* **2006**, *45*, 4864.
(35) Mai, H. X.; Zhang, Y. W.; Sun, L. D.; Yan, C. H. *Chem. Mater.* **2007**, *19*, 4514.
(36) Garcia, S. P.; Semancik, S. *Chem. Mater.* **2007**, *19*, 4016.
(37) Van der Weg, W. F.; Popma, Th. J. A.; Vink, A. T. *J. Appl. Phys.* **1985**, *57*, 5450.
(38) Sohn, K. S.; Choi, Y. Y.; Park, H. D.; Choi, H. G. *J. Electrochem. Soc.* **2000**, *147*, 2375.
(39) Riwotzki, K.; Meyssamy, H.; Kornowski, A.; Haase, M. *J. Phys. Chem. B* **2000**, *104*, 2824.
(40) Bu, W.; Chen, H.; Hua, Z.; Liu, Z.; Huang, W.; Zhang, L.; Shia, J. *Appl. Phys. Lett.* **2004**, *85*, 8.
(41) Zych, E.; Meijerink, A.; Doneg, C. M. *J. Phys.: Condens. Matter.* **2003**, *15*, 5145.

JP807527Y